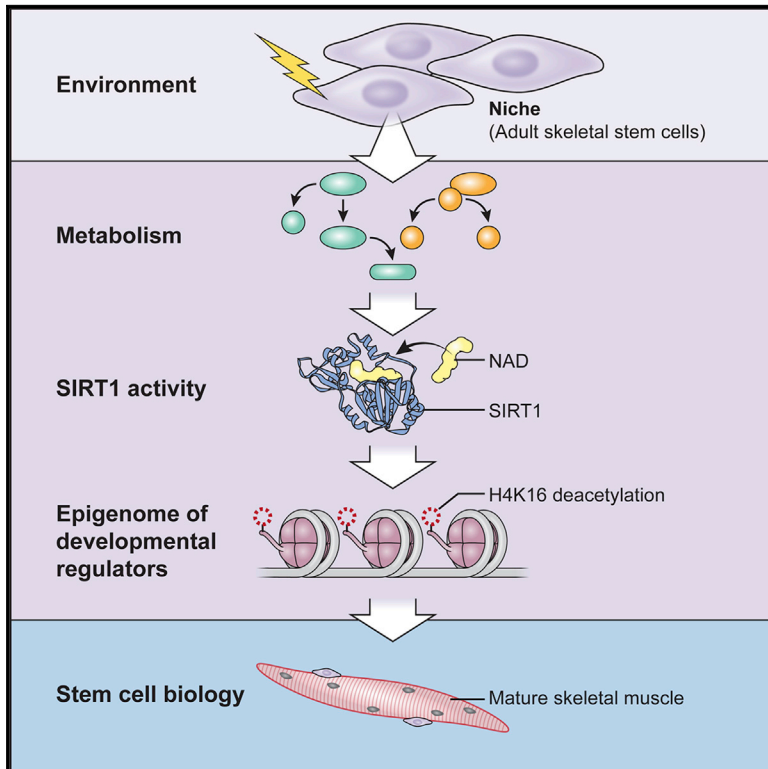


Cell Stem Cell

The NAD⁺-Dependent SIRT1 Deacetylase Translates a Metabolic Switch into Regulatory Epigenetics in Skeletal Muscle Stem Cells

Graphical Abstract



Authors

James G. Ryall, Stefania Dell'Orso, ..., Marcella Fulco, Vittorio Sartorelli

Correspondence

sartorev@mail.nih.gov

In Brief

Connecting metabolic cues to stem cell activity via epigenetic regulation: Sartorelli and colleagues show that during activation, satellite cells undergo a metabolic switch that leads to decreased intracellular NAD⁺, reduced SIRT1 deacetylase activity, elevated H4K16 acetylation, and an increase in muscle-related gene expression.

Highlights

- Satellite cells undergo a metabolic shift to glycolysis during activation
- Decreased NAD⁺ reduces SIRT1 activity and promotes H4K16 acetylation
- Ablation of SIRT1 in satellite cells leads to premature differentiation
- SIRT1 activity loss in muscles disrupts gene expression, development, and regeneration

Accession Numbers

GSE64379



The NAD⁺-Dependent SIRT1 Deacetylase Translates a Metabolic Switch into Regulatory Epigenetics in Skeletal Muscle Stem Cells

James G. Ryall,^{1,2,3} Stefania Dell'Orso,^{1,2} Assia Derfoul,¹ Aster Juan,¹ Hossein Zare,¹ Xuesong Feng,¹ Daphney Clermont,¹ Miroslav Koulis,¹ Gustavo Gutierrez-Cruz,¹ Marcella Fulco,¹ and Vittorio Sartorelli^{1,*}

¹Laboratory of Muscle Stem Cells and Gene Regulation, National Institute of Arthritis, and Musculoskeletal and Skin Diseases, National Institutes of Health, Bethesda, MD 20829, USA

²Co-first author

³Present address: Stem Cell Metabolism and Regenerative Medicine Group, Basic & Clinical Myology Laboratory, Department of Physiology, The University of Melbourne, Melbourne, VIC, 3010 Australia

*Correspondence: sartorev@mail.nih.gov

<http://dx.doi.org/10.1016/j.stem.2014.12.004>

SUMMARY

Stem cells undergo a shift in metabolic substrate utilization during specification and/or differentiation, a process that has been termed metabolic reprogramming. Here, we report that during the transition from quiescence to proliferation, skeletal muscle stem cells experience a metabolic switch from fatty acid oxidation to glycolysis. This reprogramming of cellular metabolism decreases intracellular NAD⁺ levels and the activity of the histone deacetylase SIRT1, leading to elevated H4K16 acetylation and activation of muscle gene transcription. Selective genetic ablation of the SIRT1 deacetylase domain in skeletal muscle results in increased H4K16 acetylation and deregulated activation of the myogenic program in SCs. Moreover, mice with muscle-specific inactivation of the SIRT1 deacetylase domain display reduced myofiber size, impaired muscle regeneration, and derepression of muscle developmental genes. Overall, these findings reveal how metabolic cues can be mechanistically translated into epigenetic modifications that regulate skeletal muscle stem cell biology.

INTRODUCTION

Cellular energy is generated via oxidative-phosphorylation (OXPHOS) in the mitochondria and glycolysis in the cytoplasm. In addition to providing a steady supply of energy, the metabolic state of the cell can influence the epigenome and alter gene expression. This flow of information is afforded by intermediate metabolites that directly or indirectly affect the activity of chromatin-modifying enzymes involved in regulating chromatin dynamics and transcription (Katada et al., 2012; Lu and Thompson, 2012). Cellular substrate and oxygen availability, as well as energy demand, determine which metabolic pathway is used to generate ATP. Under reduced oxygen tension, ATP is generated via anaerobic glycolysis, whereas in aerobic conditions ATP is

produced mainly via OXPHOS, a process involving the breakdown of substrates to acetyl-CoA, and leading to the production of the reduced form of nicotinamide adenine dinucleotide (NAD⁺) NADH via the tricarboxylic cycle (TCA). Compared to OXPHOS, glycolysis is an inefficient method to generate ATP. However, it provides a number of important advantages for cells, including the ability to rapidly generate ATP in response to acute changes in energy demand, as well as generating the necessary glycolytic intermediates for the biosynthesis of new macromolecules essential for proliferating cells (Lunt and Vander Heiden, 2011; Ryall, 2013; Shyh-Chang et al., 2013).

The enzymatic activity of sirtuin 1 (SIRT1), a member of the class III deacetylase family (Guarente, 2000; Michan and Sinclair, 2007), is regulated by the free concentration of the intermediate metabolite NAD⁺ (Imai et al., 2000). Whereas a plethora of nonhistone proteins are deacetylated by SIRT1 (Houtkooper et al., 2012; Rodgers et al., 2005), acetylated lysine 16 of histone H4 (H4K16ac) serves as a preferred SIRT1 histone substrate (Vaquero et al., 2004). Even though regulation of sirtuin enzymology is energy demanding and complex (Sauve and Youn, 2012), it establishes, in principle, a rapid and finely tunable biochemical system through which changes in metabolism can be effectively converted into distinct epigenetic states and gene expression patterns.

Satellite cells (SCs) are skeletal muscle stem cells required for muscle growth and tissue repair (Brack and Rando, 2012; Tajbakhsh, 2009; Yin et al., 2013). Following intense proliferation associated with mouse postnatal muscle growth, SCs enter a quiescent state, representing 3%–5% of the total number of adult muscle fiber nuclei (Yin et al., 2013). In response to muscle injury, the niche is remodeled and quiescent SCs enter the cell cycle (become activated). Activated SCs are characterized by the presence of the muscle-specific transcription factor MyoD, and give rise to committed proliferating muscle precursors which, upon expression of the myogenic transcription factor Myogenin, differentiate and fuse to repair damaged muscles (Tajbakhsh, 2009; Yin et al., 2013). Due to changes in requirements placed on SCs during the transition from quiescence to activation, significant differences in the underlying metabolism of these cellular states are likely to occur. Here we describe a metabolic shift from fatty acid (FA) and pyruvate oxidation in quiescent SCs to increased glycolysis and glutaminolysis during SC activation and proliferation. In addition, we document that this process of

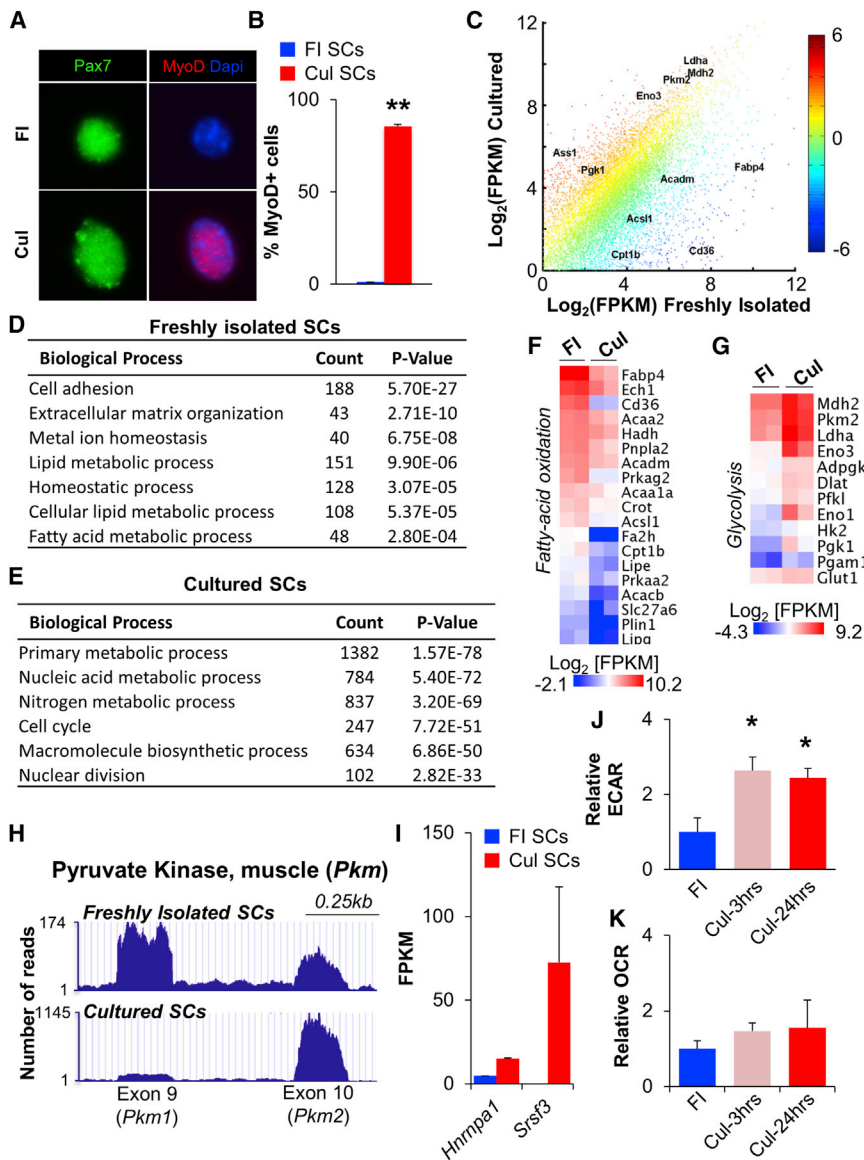


Figure 1. Satellite Cells Undergo a Switch from Oxidative to Glycolytic Metabolism following Culture in Growth Media

(A) Immunofluorescent analyses of freshly isolated (FI, quiescent) and cultured (Cul, activated) SCs with Pax7 (green) and MyoD (red) antibodies. 4', 6-Diamidino-2-phenylindole stain identifies nuclei. (B) Quantification of MyoD⁺ SCs in FI and Cul cell populations.

(C) RNA-seq scatter plot with key metabolic regulators indicated. Each data point represents the mean Log₂[FPKM] from two independent biological replicates with color indicating the relative fold change in gene expression.

(D and E) Gene ontology analyses of RNA-seq revealed an enrichment of biological processes specific to FI SCs (D) or Cul SCs (E). The number of genes enriched by greater than 1.5-fold is indicated under the "Count" column.

(F and G) Heat maps indicating absolute gene expression (Log₂[FPKM]) of specific metabolic regulators in FI and Cul SCs. Each gene listed had a mean fold change of greater than 1.5.

(H) RNA-seq traces (UCSC genome browser) for *Pkm* 1 and 2 isoforms in FI and Cul WT SCs.

(I) Expression of the *Pkm* splice regulators *Hnrmpa1* and *Srsf3* in FI and Cul SCs.

(J and K) Cellular bioenergetics in SCs during culture in growth conditions were evaluated with Seahorse XF96 bioanalyzer. Glycolysis (ECAR) was increased 2.5-fold in Cul-3 hr and Cul-24 hr SCs (J), whereas basal oxygen consumption (OCR) was not different between FI, Cul-3 hr, or Cul-24 hr SCs (K). Data are presented as mean ± SEM. *p < 0.05 and **p < 0.01 (FI SCs versus Cul SCs).

SC metabolic reprogramming is associated with a decrease in the intracellular NAD⁺/NADH ratio, reduced SIRT1-mediated deacetylation of H4K16ac, and activation of the myogenic program. SCs derived from mice with muscle-specific inactivation of the *Sirt1* deacetylase domain (*Sirt1*^{mkO} mice) display increased H4K16ac and deregulated activation of the myogenic program. Finally, *Sirt1*^{mkO} mice have reduced myofiber size, exhibit impaired muscle regeneration, and reveal a depression of several muscle developmental genes.

RESULTS

Quiescent Skeletal Muscle Stem Cells Undergo a Switch from Fatty Acid and Pyruvate Oxidation to Glycolysis during Culture in Growth-Permissive Conditions

To analyze transcriptomes of quiescent and proliferating SCs, we used fluorescence-activated cell sorting (FACS) followed by RNA sequencing (RNA-seq). FACS isolation of SCs from two

SCs were immediately processed following the completion of sorting, whereas an aliquot of FACS-isolated SCs were cultured (Cul) on collagen-coated plates in growth media for 48 hr. Quiescent SCs are Pax7⁺/MyoD⁻, whereas activated SCs are Pax7⁺/MyoD⁺ (Kuang et al., 2008); therefore, we analyzed aliquots of FI or Cul SCs and confirmed them to be Pax7⁺/MyoD⁻ and Pax7⁺/MyoD⁺, respectively (Figures 1A and 1B).

RNA-seq results from FI and Cul SCs identified a large number of differentially regulated genes (Figure 1C and Table S1). Gene ontology (GO) analyses of biological processes highlighted the expected changes following the transition from quiescence to proliferation, with adhesion- and homeostatic-related terms enriched in FI SCs (Figures 1D and S1E and Table S1), and cell-cycle and nuclear division terms enriched in Cul SCs (Figures 1E and S1F and Table S1). Moreover, the two markers of SC quiescence Sprouty 1 (*Spry1*, Shea et al., 2010) and calcitonin receptor (*Calcr*, Fukada et al., 2007) were enriched in FI SCs (Table S1). In addition, changes in a number of genes encoding

month-old C57BL/6 mouse hindlimb muscles was based on selection of α 7-integrin⁺, Hoechst⁺, PI⁻ and Lin⁻ (CD11/CD31/CD45/Sca1) cells (modified from Kuang et al., 2007; Figures S1A–S1D available online). Freshly isolated (FI)

for metabolic regulators were observed in the transition from quiescence to proliferation (Figures 1C and 1E). The expression of genes corresponding to proteins that regulate FA metabolic processes and lipid catabolic processes was downregulated (Figure 1F), whereas that of genes regulating glucose catabolic processes, glutaminolysis, macromolecular biosynthesis (including the pentose phosphate pathway, PPP) and amino-acid transporters was increased in Cul SCs (Figure 1G; Figures S1G and S1H). Indicating that transcriptional activation of the glycolytic program was not simply the result of in vitro culture conditions, transcription of a similar subset of genes was increased in proliferating SCs derived from regenerating skeletal muscle (Liu et al., 2013). In addition to a global upregulation of genes encoding glycolytic enzymes, we observed that the muscle pyruvate kinase 2 (Pkm2) isoform, known to promote “aerobic-glycolysis” (or the Warburg effect), predominated over its alternative spliced isoform Pkm1 in Cul SCs (Figure 1H). Consistently, expression of *Hnnpa1* and *Srsf3*, two mediators of Pkm alternative splicing, was also increased (Figure 1I).

Whereas these results are suggestive of a shift in substrate uptake and utilization during the switch from quiescent to proliferating SCs, to directly confirm that glycolysis was elevated in Cul SCs, we used the Seahorse extracellular flux bioanalyzer to examine both the basal oxygen consumption rate (OCR, an indicator of mitochondrial oxidative activity) and the basal extracellular acidification rate (ECAR, a marker of glycolysis). We observed a 2.5-fold increase in the ECAR (i.e., increased glycolysis) in both Cul-3 hr and Cul-24 hr SCs, compared to FI SCs (Figure 1J). However, there was no difference in the basal mitochondrial OCR between FI SCs and the two stages of cultured SCs examined (Figure 1K). Because a recent study identified an increase in mitochondria following 60 hr of SC activation in vivo (Rodgers et al., 2014), we examined mitochondrial content in FI and Cul SCs. Similar to that observed in vivo, there was a progressive increase in Mitotracker fluorescence in Cul SCs during 48 hr of culture (Figure S2A) and an enrichment of genes known to regulate the TCA cycle (Figure S2B). These results suggest that Cul SCs preferentially increase their glycolytic rate, despite increasing their mitochondrial content. This observation is reminiscent of mouse epiblast stem cells, which have larger and more complex mitochondria than mouse embryonic stem cells, and yet exhibit a lower level of oxygen consumption (Zhou et al., 2012).

Altogether, these results indicate that Cul SCs undergo a shift away from FA oxidation, toward glycolysis, glutaminolysis, and activation of the PPP for macromolecule biosynthesis.

SIRT1 Deacetylase Activity and NAD⁺ Levels Are Elevated in Quiescent Compared to Activated Skeletal Muscle Stem Cells

An increased reliance upon oxidative metabolism has been proposed to lead to elevated SIRT1 deacetylase activity, either via changes in absolute SIRT1 levels or changes in the NAD⁺/NADH ratio (Guarente, 2011; Ryall, 2012; Figure 2A). The shift away from FA oxidation in Cul SCs was associated with a 1.5-fold decrease in the expression of both *Sirt1* and the NAD⁺-generating enzyme *Nampt*, as measured by qPCR (Figure 2B). However, despite this decline, SIRT1 protein was readily detected and predominantly localized to the nucleus of both FI

and Cul SCs (Figure 2C). Global H4K16ac, a substrate for SIRT1-mediated deacetylation (Vaquero et al., 2004), was examined in SCs associated with freshly isolated single extensor digitorum longus (EDL) muscle fibers, and fibers that had been cultured in growth media for 3 or 20 hr (Figures 2D and 2E). Single myofiber isolation permits SCs to remain attached to the myofiber and, thus, to maintain their position in the physiological niche between the basal lamina and the sarcolemma (Collins and Zammit, 2009). Myofiber-associated SCs cultured in growth media for 3 or 20 hr displayed a 7- and 16-fold increase in the median level of H4K16ac, compared to SCs on freshly isolated myofibers (Figures 2D and 2E), respectively. Thus, while SIRT1 protein was observed in the nucleus of Cul SCs, global H4K16ac was strongly elevated during the early stages of culture, suggesting a possible regulation of SIRT1 activity. Because SIRT1 deacetylase activity is dependent upon NAD⁺ supply (Imai et al., 2000), we used FACS-isolated SCs to examine NAD⁺ levels. Whereas NADH was undetectable in both FI and Cul SCs, the amount of total NAD⁺ was 10-fold higher in FI than Cul SCs (Figure 2F). Therefore, H4K16 deacetylation, a proxy for SIRT1 deacetylase activity, and NAD⁺ were elevated in FI SCs, and reduced in Cul SCs.

Metabolic Reprogramming of Proliferating Muscle Cells to Oxidative Phosphorylation Leads to a SIRT1-Dependent Repression of MyoD

In contrast to glucose, for galactose to be used as an energy substrate it must first be converted to glucose-6-phosphate in an ATP-consuming reaction, leading to no net gain in ATP via glycolysis (Gohil et al., 2010). Cells incubated with galactose must therefore rely on OXPHOS to generate ATP (Figure 3A). To test whether metabolic reprogramming affects the NAD⁺/NADH ratio, H4K16ac, and muscle gene expression, we used myogenic C2C12 cells. Although C2C12 cells do not recapitulate all the features of SCs, they nonetheless retain some shared characteristics. C2C12 cells incubated for 3 hr in growth media containing galactose (10 mM) exhibited significantly reduced glycolysis (as indicated via decreased ECAR) and increased oxygen consumption (measured as OCR) compared to cells incubated in growth media containing glucose (25 mM; Figure 3B). Culturing C2C12 cells in growth media containing galactose resulted in an increase of NAD⁺, with a concomitant decrease in NADH, and a net 2.5-fold increase in the NAD⁺/NADH ratio of cells (Figures 3C and 3D). We confirmed that incubation with galactose did not impair ATP generation (and activate starvation pathways), and in fact resulted in elevated levels of ATP (Figure 3E).

The results presented in the preceding paragraphs indicate that a switch from oxidative phosphorylation to glycolysis accompanying SC activation has the potential to modulate the deacetylase activity of SIRT1 via decreased NAD⁺ availability. To directly test this possibility, we transduced C2C12 cells with a SIRT1 shRNA retrovirus. The reduced SIRT1 protein levels in these cells were associated with increased MyoD expression, elevated global H4K16ac, and a reduced rate of proliferation (Figures S3A and S3B). Consistent with a role of SIRT1 in mediating these phenomena, the addition of increasing concentrations of the SIRT1 inhibitor nicotinamide (NAM) to proliferating C2C12 cells similarly led to an increase in global

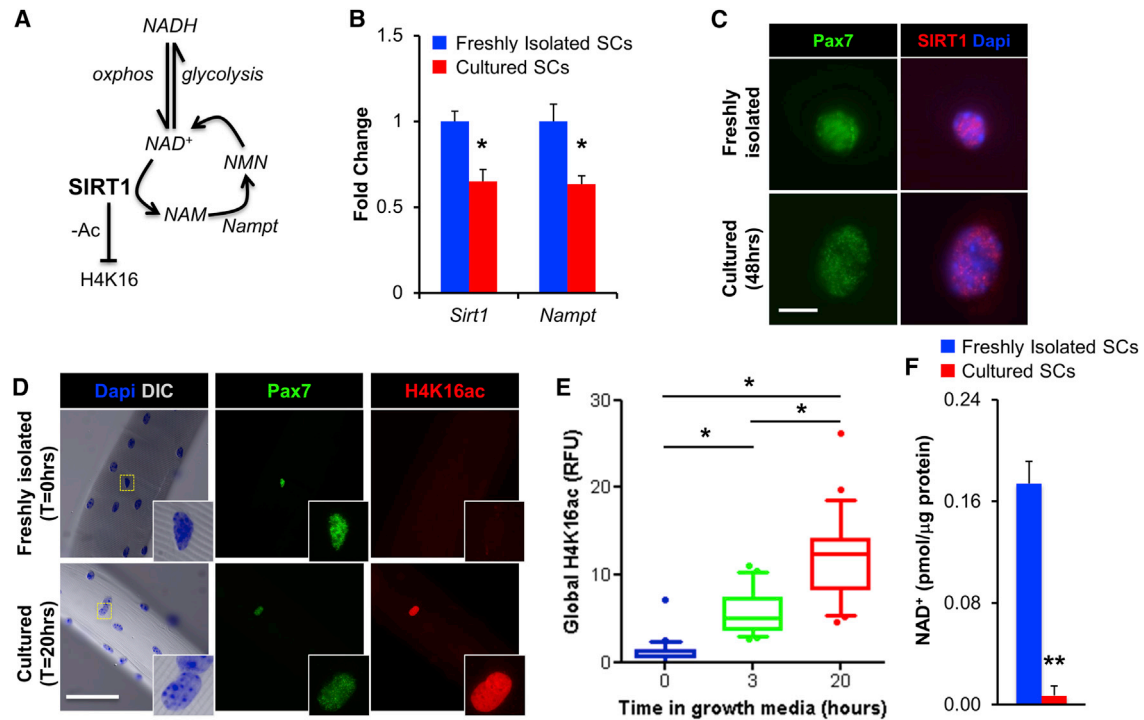


Figure 2. The Histone Deacetylase Activity of SIRT1 Is Reduced following Satellite Cell Activation

(A) Scheme depicting how the deacetylase activity of SIRT1 is dependent on both metabolic processes ($\text{NAD}^+ \leftrightarrow \text{NADH}$) and the NAD^+ salvage pathway ($\text{NAD}^+ \leftrightarrow \text{NAM}$). H4K16, histone H4 lysine 16; NAD, nicotinamide adenine dinucleotide; NAM, nicotinamide; NMN, nicotinamide mononucleotide nucleosidase; Nampt, nicotinamide phosphoribosyltransferase.

(B) *Sirt1* and *Nampt* expression in FI and Cul SCs, as measured by qPCR ($n = 3$).

(C) SIRT1 and Pax7 immunofluorescence of FACS-isolated FI and Cul SCs. White scale bar represents 5 μm .

(D) Pax7 and H4K16ac immunofluorescence of SCs on freshly isolated single muscle fibers. White scale bar represents 50 μm ; inset is magnified by a magnitude of four.

(E) Quantification of relative fluorescence (RFU) in SCs labeled for H4K16ac ($n = 2$ mice, >50 fibers/time point). Results are presented as box-and-whisker plots, with a significant difference indicated when the median \pm 95% CI does not overlap.

(F) Total NAD levels in FI and Cul SCs (48 hr in growth media, $n = 3$). Data are presented as mean \pm SEM, * $p < 0.05$ and ** $p < 0.01$ (FI SCs versus Cul SCs).

H4K16ac and MyoD expression (Figure S3C). C2C12 cells cultured in galactose (Gal) exhibited a progressive decline in the expression of MyoD protein levels starting at 3 hr and further decreasing at 6 hr (Figure 3F, compare lanes 5–6, 9–10). Importantly, the galactose-induced decline in MyoD protein was abrogated by SIRT1 shRNA (Figure 3F, compare lanes 6 and 8, and 10 and 12), indicating a role for SIRT1 at the nexus between changes in cellular metabolism and expression of the master regulator MyoD.

Ablation of the SIRT1 Deacetylase Domain Leads to Premature Differentiation of Skeletal Muscle Stem Cells

To investigate whether SIRT1 influences SC biology *in vivo*, we generated a Pax7-specific *Sirt1* knockout mouse (*Sirt1*^{muscle KO}) by crossing mice containing the Cre-recombinase under the control of the Pax7 locus (Pax7-Cre, Keller et al., 2004) with mice containing a modified *Sirt1* gene where exon 4 (located within the catalytic deacetylase domain) is flanked by loxP sites (SIRT1 floxed mice, Li et al., 2007). The floxed alleles were detected in genomic DNA isolated from skeletal muscle of Cre-negative (WT) mice, while the Δ^{ex4} alleles were detected in the presence of Cre-recombinase in *Sirt1*^{muscle KO} mice (Figure 4A, top). A band

corresponding to the SIRT1 protein (Figure 4A bottom, arrow) was lost and, concomitantly, a slightly faster migrating band corresponding to SIRT1 Δ^{ex4} appeared (Figure 4A bottom, arrowhead), specifically in the skeletal muscles of *Sirt1*^{muscle KO} mice, compared with WT. Freshly isolated single EDL muscle fibers were obtained from WT and *Sirt1*^{muscle KO} mice, stained with Pax7 to identify SCs and costained with H4K16ac-specific antibodies. Whereas WT myofibers had a tight distribution of SCs expressing low levels of global H4K16ac, SCs on *Sirt1*^{muscle KO} myofibers had a wider distribution of H4K16ac levels, such that there was a 2-fold increase in the median level of global SC H4K16ac (Figures 4B and 4C). These results indicate that, in SCs, SIRT1 is required to maintain H4K16 in a deacetylated state. Moreover, the percentage of Pax7⁺/MyoD⁺ SCs on *Sirt1*^{muscle KO} fibers was increased (Figures 4D, 4E, and S3D). In light of these findings, we asked whether *Sirt1*^{muscle KO} SCs may also undergo premature differentiation and, if so, whether this is a cell-autonomous phenomenon. FACS-isolated SCs were cultured for 24 hr. Compared to WT cells, *Sirt1*^{muscle KO} SCs mice exhibited an overt spindle-like, elongated morphology, indicative of early differentiation (Figure 4F).

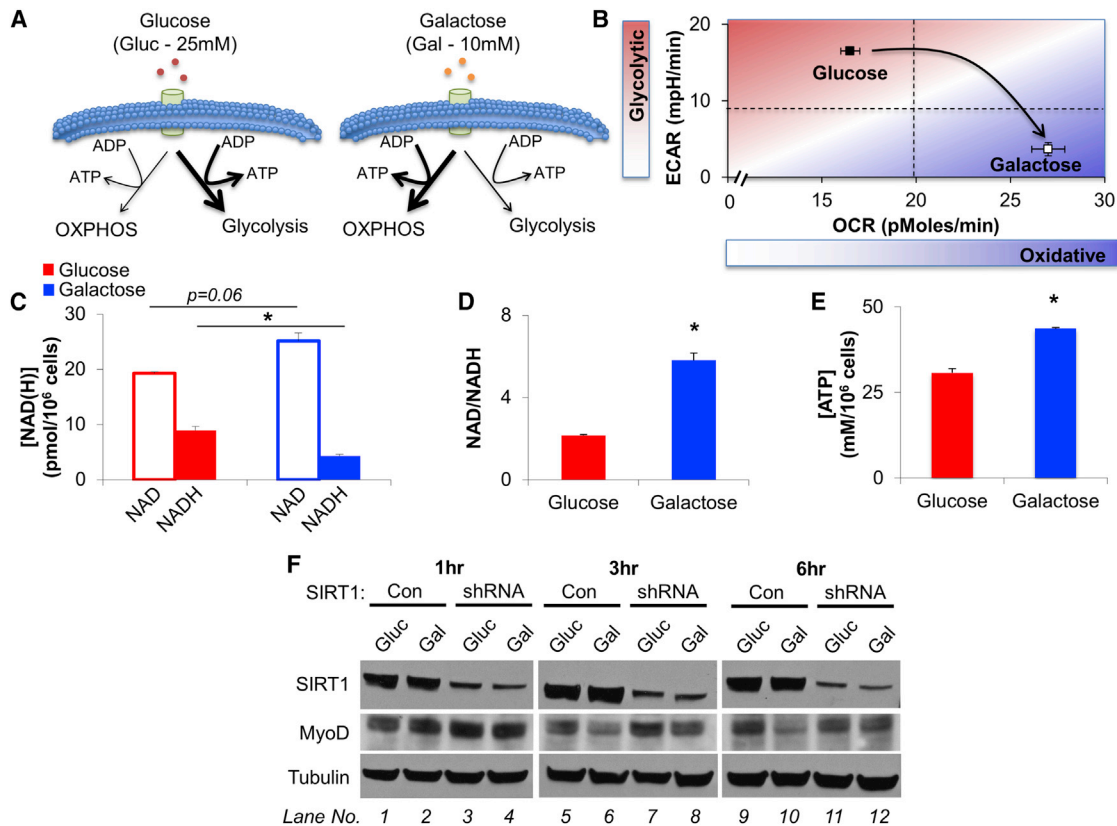


Figure 3. A Forced Shift to Oxidative Metabolism Increases NAD⁺ Levels and Reduces MyoD in Control but Not SIRT1 shRNA Cells

(A) Schematic depicting how glucose is used to preferentially generate ATP via glycolysis. Replacing glucose with galactose forces cells to shift to predominantly use OXPHOS for the generation of ATP.

(B) C2C12 basal cellular bioenergetics were analyzed on a Seahorse XF96 bioanalyzer during culture in either glucose or galactose based growth media (n = 15 replicates/group).

(C and D) Culturing C2C12 cells in galactose-based growth media increases the amount of NAD⁺, at the expense of NADH such that there was a 3-fold increase in the NAD/NADH ratio (n = 3).

(E) Replacing glucose with galactose in C2C12 growth media led to an elevation in ATP levels (n = 3).

(F) Incubating C2C12 cells with galactose instead of glucose for 3 and 6 hr results in a decrease in MyoD in WT (compare lanes 5–6, and 9–10), but not SIRT1 shRNA C2C12 cells (compare lanes 7–8, and 11–12). Data are presented as mean ± SEM. *p < 0.05.

SIRT1 Regulates H4K16 Acetylation and Expression of Selected Genes

To thoroughly investigate the global impact of inactivating the SIRT1 deacetylase activity on the transcriptome, we performed RNA-seq on SCs derived from WT or *Sirt1*^{mkKO} mice at several stages of myogenesis, including quiescence (FI), activation (Cul), and early differentiation (Diff).

In FI *Sirt1*^{mkKO} SCs, 361 genes were downregulated compared to FI WT SCs (Table S2). On the other hand, transcripts corresponding to 287 genes were upregulated (Figure 5A and Table S2). Among the upregulated genes in FI *Sirt1*^{mkKO} SCs were those for muscle-specific myosin light chain kinase 2 (*Mylk2*; Figure 5B; Table S2), myosin light chain phosphorylatable (*Mylpf*), the skeletal muscle proteoglycan biglycan (*Bgn*), and the skeletal muscle-specific ryanodine receptor 1 (*Ryr1*, Table S2). Expression of these genes is physiologically observed in differentiated skeletal muscle cells. Other upregulated transcripts corresponded to the BMP inhibitors chordin (*Chrd*) and follistatin (*Fst*), known to play functional roles in

SC proliferation and differentiation (Jeong et al., 2013; Ono et al., 2011), and transcription factors eyes-absent 1 (*Eya1*-required for somitic myogenesis, Grifone et al., 2007) and *Foxo3* (Table S2; Dentice et al., 2010). Overall, these findings indicate a propensity of FI *Sirt1*^{mkKO} SCs to activate genes physiologically expressed in activated/differentiating SCs. In Cul *Sirt1*^{mkKO} SCs, 322 genes were downregulated, whereas 253 transcripts were upregulated (Figure 5C; Table S2). *Bgn*, a transcript upregulated in FI *Sirt1*^{mkKO} SCs, continued to be increased, and transcripts for the decorin (*Dcn*) gene, whose expression is increased during muscle regeneration of *mdx* mice (Abe et al., 2009) were augmented (Table S2). Transcripts corresponding to the H19 long noncoding (lnc) RNA were also increased (Figure 5D). Processing of H19 lnc RNA generates miR-675-3p and -5p, two microRNAs induced and required for skeletal muscle differentiation (Dey et al., 2014). In *Sirt1*^{mkKO} SCs induced to differentiate, 177 genes were downregulated (Table S2) and 757 gene transcripts were increased (Figure 5E and Table S2). The upregulated transcripts included actins,

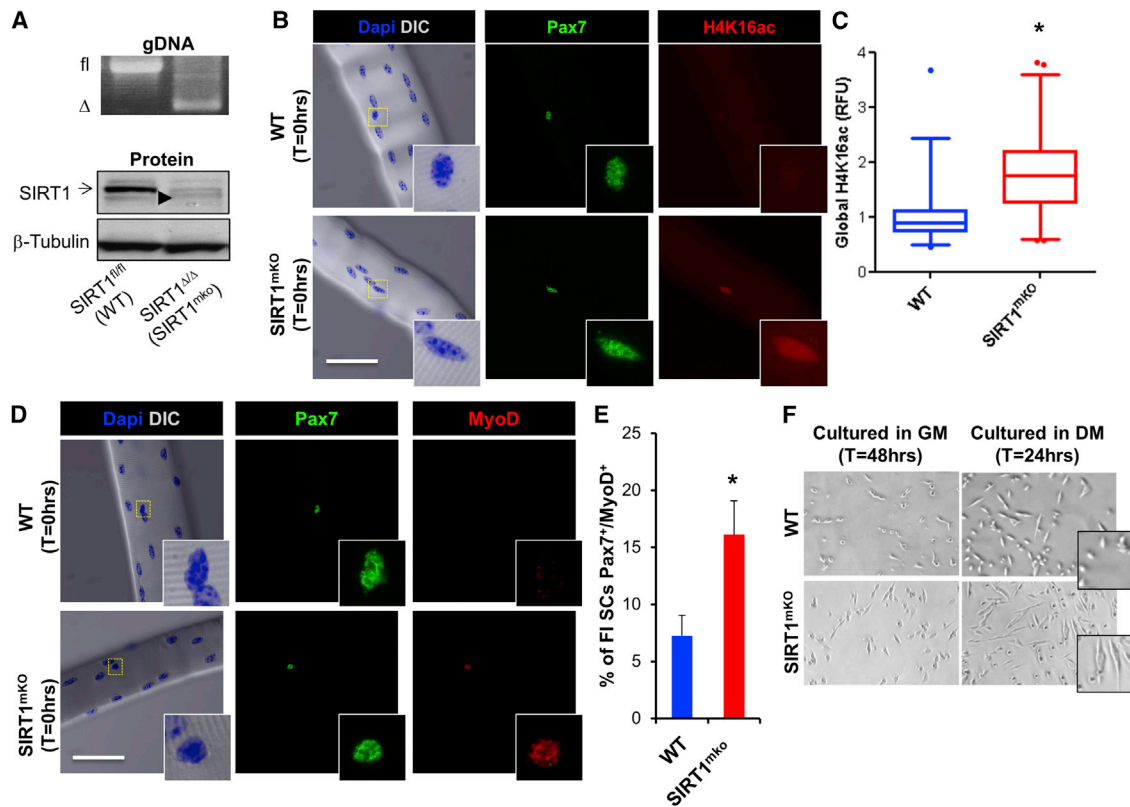


Figure 4. Ablation of the Catalytic Domain of SIRT1 Results in Increased Global H4K16ac and Precocious Activation/Differentiation of SCs

(A) Skeletal muscle from WT mice demonstrated the presence of the *Sirt1* floxed allele (fl, top) and detectable levels of SIRT1 protein (arrow, bottom), whereas *Sirt1*^{mko} muscle contained the *Sirt1*^{Δex4} allele (Δ, top) and ablation of SIRT1 protein. A small level of SIRT1^{Δex4} protein was detectable in the skeletal muscle of *Sirt1*^{mko} mice (arrowhead, bottom).

(B and C) In *Sirt1*^{mko} mice, quiescent SCs (identified as Pax7⁺) exhibited a 2-fold increase in global H4K16ac, compared to WT mice, as determined via relative fluorescence (RFU) in SCs labeled for H4K16ac (n = 2 mice, >50 fibers/time point). White scale bar represents 50 μm; inset is magnified by a magnitude of four. Results are presented as box-and-whisker plots (fifth to 95th percentiles), with a significant difference indicated when the median ± 95% CI does not overlap.

(D and E) MyoD and Pax7 staining (n = 2 mice, >50 fibers/time point) of fiber-associated *Sirt1*^{mko} SCs. Data are presented as mean ± SEM, *p < 0.05.

(F) DIC images of SCs isolated from WT and *Sirt1*^{mko} mice during proliferation in growth media (GM, 48 hr), or early differentiation in differentiation media (24 hr DM). Note the overt spindle-like, elongated morphology of SCs from *Sirt1*^{mko} mice indicating premature differentiation.

myosins, and troponins (Table S2). Transcription factors influencing different aspects of myogenesis, such as *Myog* (Figure 5F), *Mef2a-d*, *Eya4*, *Nfatc*, *Nfix*, and *Smad3* were also increased (Table S2). The H19 lncRNA, upregulated in Cul (Figure 5D), was also increased in *Sirt1*^{mko} SCs induced to differentiate (Figure S5C). Of particular interest, transcripts typically expressed in either embryonic muscle and/or upregulated during muscle regeneration including the embryonic myosin heavy chain isoform (*Myh3*), filamin C (*Flnc*), and brain expressed 1 (*Bex1*) were increased in *Sirt1*^{mko} SCs (Goetsch et al., 2005; Koo et al., 2007; Weydert et al., 1987; Table S2; Figure 7G).

Of all histone lysines, acetylation of H4K16 profoundly alters chromatin structure by disrupting formation of the 30 nm chromatin fibers and preventing cross-fiber formation (Shogren-Knaak et al., 2006). Accordingly, subtle enrichment of H4K16ac significantly and positively affects transcription (Taylor et al., 2013). To correlate transcription and H4K16ac enrichment, ~1 × 10⁶ SCs derived from seven to eight WT or *Sirt1*^{mko} mice were used for chromatin immunoprecipitation sequencing (ChIP-seq) after immunoprecipitation with an

H4K16ac antibody. H4K16 acetylation was observed to predominantly occur at and around the transcriptional start site (TSS) and was higher in Cul SCs compared to FI SCs (Figure 6A). Moreover, there was a positive correlation between H4K16ac and gene expression, so that the genes with the highest expression were also the most H4K16 acetylated in both Cul SCs (Figure 6B) and FI SCs (Figure S4A). We addressed the genome-wide role of SIRT1 on H4K16ac and gene expression by correlating H4K16ac ChIP-seq and RNA-seq datasets from WT and *Sirt1*^{mko} SCs. Global H4K16ac at the 253 upregulated genes in Cul *Sirt1*^{mko} SCs was already increased in FI *Sirt1*^{mko} SCs (Figure 6C). Similarly, H4K16ac at the 757 genes whose transcription was increased in *Sirt1*^{mko} SCs induced to differentiate was also increased in FI *Sirt1*^{mko} SCs, being positioned at an intermediate H4K16ac level between that observed in FI and Cul WT SCs (Figure 6D). Of the 287 genes upregulated in FI *Sirt1*^{mko} SCs, one-third (88/287, 30%, Table S3) displayed significantly increased H4K16ac (Figure 6E). However, the vast majority of H4K16ac was found to occur at genes whose transcription

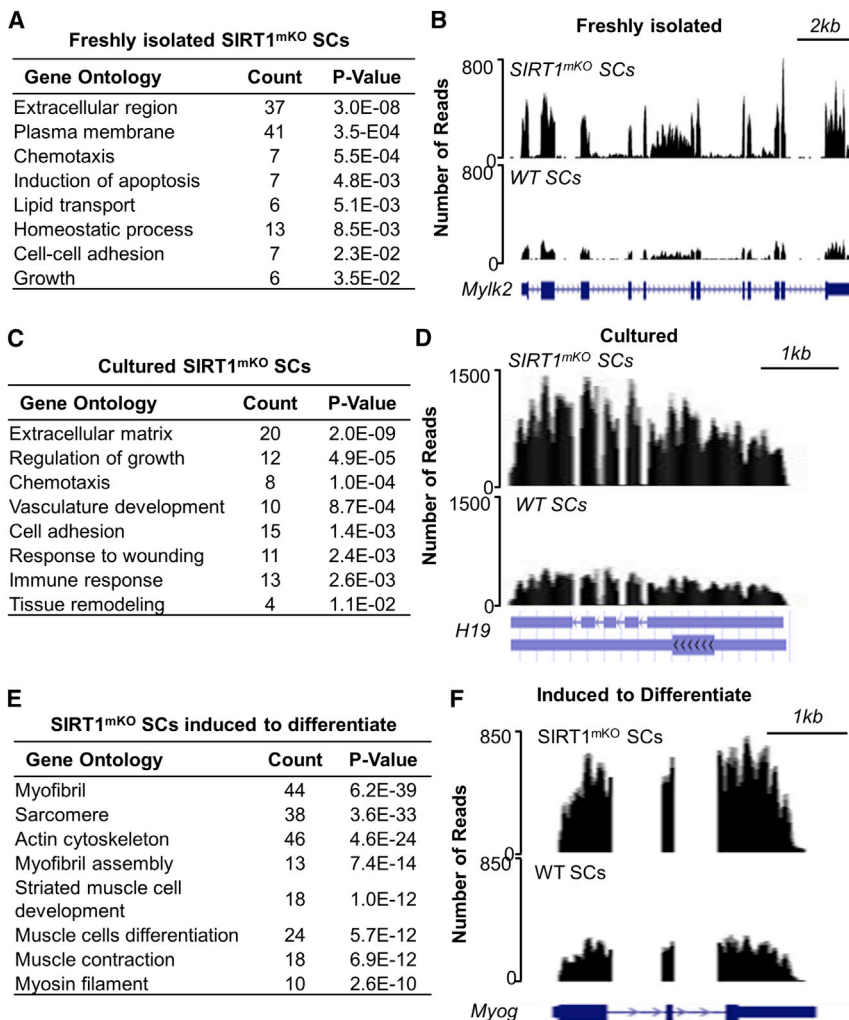


Figure 5. Ablation of the SIRT1 Catalytic Domain Leads to Modifications in Gene Expression in Both Freshly Isolated and Cultured Satellite Cells

(A) Gene ontology (GO) of genes upregulated in FI *Sirt1*^{mkO} SCs. (B) RNA-seq profiles (UCSC genome browser) of the *Mylk2* gene in FI WT SCs (bottom) and FI *Sirt1*^{mkO} SCs (top). (C) GO of genes upregulated in Cul *Sirt1*^{mkO} SCs. (D) RNA-seq profiles of the *H19* gene in Cul WT SCs (bottom) and Cul *Sirt1*^{mkO} SCs (top). (E) GO of genes upregulated in *Sirt1*^{mkO} SCs induced to differentiate (24hrs DM). (F) RNA-seq profiles of the *Myog* gene in WT (bottom) and *Sirt1*^{mkO} SCs (top) induced to differentiate. RNA-seq experiments were done with either three (FI SCs) or two (Cul and Differentiating SCs) biological replicates.

Metabolic Reprogramming of Skeletal Muscle Stem Cells Leads to a SIRT1-Dependent Delay in H4K16ac Acquisition and MyoD Expression

To further examine the link between metabolism, H4K16ac and SC activation, we used isolated single fibers from WT and *Sirt1*^{mkO} mice and incubated them for 20 hr in either glucose- (25 mM) or galactose- (10 mM) based growth media (Figure S7). Similarly to what observed in C2C12 cells (Figure 3), SCs from WT mice incubated in galactose-supplemented media exhibited a reduction in global H4K16ac and MyoD expression, compared to SCs incubated in glucose

media (Figures S7A and S7C). In contrast, SCs from *Sirt1*^{mkO} mice did not exhibit any appreciable difference in global H4K16ac or MyoD expression in either glucose or galactose media (Figures S7B and S7D). Overall, these results provide evidence for a direct link between a change in metabolism and SC activation and support a role for SIRT1 in this process, downstream of the change in metabolism.

was not concomitantly increased (Figure 6E). In Cul *Sirt1*^{mkO} SCs, 85 of the 253 upregulated genes (33%, Table S3) had increased H4K16ac (Figure 6E), and 275 out of the 757 upregulated genes (36%, Table S3) in *Sirt1*^{mkO} SCs were induced to differentiate and manifested increased H4K16ac when assayed in FI *Sirt1*^{mkO} SCs (Figure 6E). To directly analyze a link between SIRT1, H4K16ac and gene expression, we performed SIRT1 ChIP-seq in FI and Cul SCs (Table S4). Examples of selected genes are illustrated in genome browser screenviews for SIRT1 ChIP-seq, H4K16ac ChIP-seq as well as RNA-seq traces (Figures 6F and 6G; Figures S4 and S5). SIRT1 was enriched at the *Mylk2*, *H19*, and *Myog* loci in FI but absent in Cul SCs, its enrichment negatively correlating with H4K16ac and gene transcription (Figures 6F and 6G). H4K16 acetylation and SIRT1 enrichment at the *Mylk2* and *Myog* were validated using ChIP-qPCR (Figure S6). These findings are in agreement with our previous results indicating a repressive role of SIRT1 for *Myog* expression (Fulco et al., 2003). Overall, the results described in this paragraph indicate that while SIRT1 regulates the H4K16ac status at several thousand loci, its deletion only permits the expression of a few hundred genes.

media (Figures S7A and S7C). In contrast, SCs from *Sirt1*^{mkO} mice did not exhibit any appreciable difference in global H4K16ac or MyoD expression in either glucose or galactose media (Figures S7B and S7D). Overall, these results provide evidence for a direct link between a change in metabolism and SC activation and support a role for SIRT1 in this process, downstream of the change in metabolism.

Ablation of SIRT1 Deacetylase Activity Leads to Developmental and Regenerative Defects in *Sirt1*^{mkO} Mice

To determine the effects of *Sirt1* ablation in skeletal muscle, we investigated phenotypic changes in *Sirt1*^{mkO} mice during both development and regeneration. *Sirt1*^{mkO} mice were initially smaller than littermate controls (Figure 7A) and had reduced *Pax7* gene and protein expression (Figures 7B and 7C). In addition, at postnatal day 9 (P9), skeletal muscles from *Sirt1*^{mkO} mice exhibited smaller fiber cross-sectional areas (CSA, Figures 7D and 7E). By day P14, the body mass of *Sirt1*^{mkO} mice became indistinguishable from littermate controls (data not shown). Interestingly, it is approximately at P14 that SCs gradually start reducing their proliferation to enter quiescence at P21 (Chang

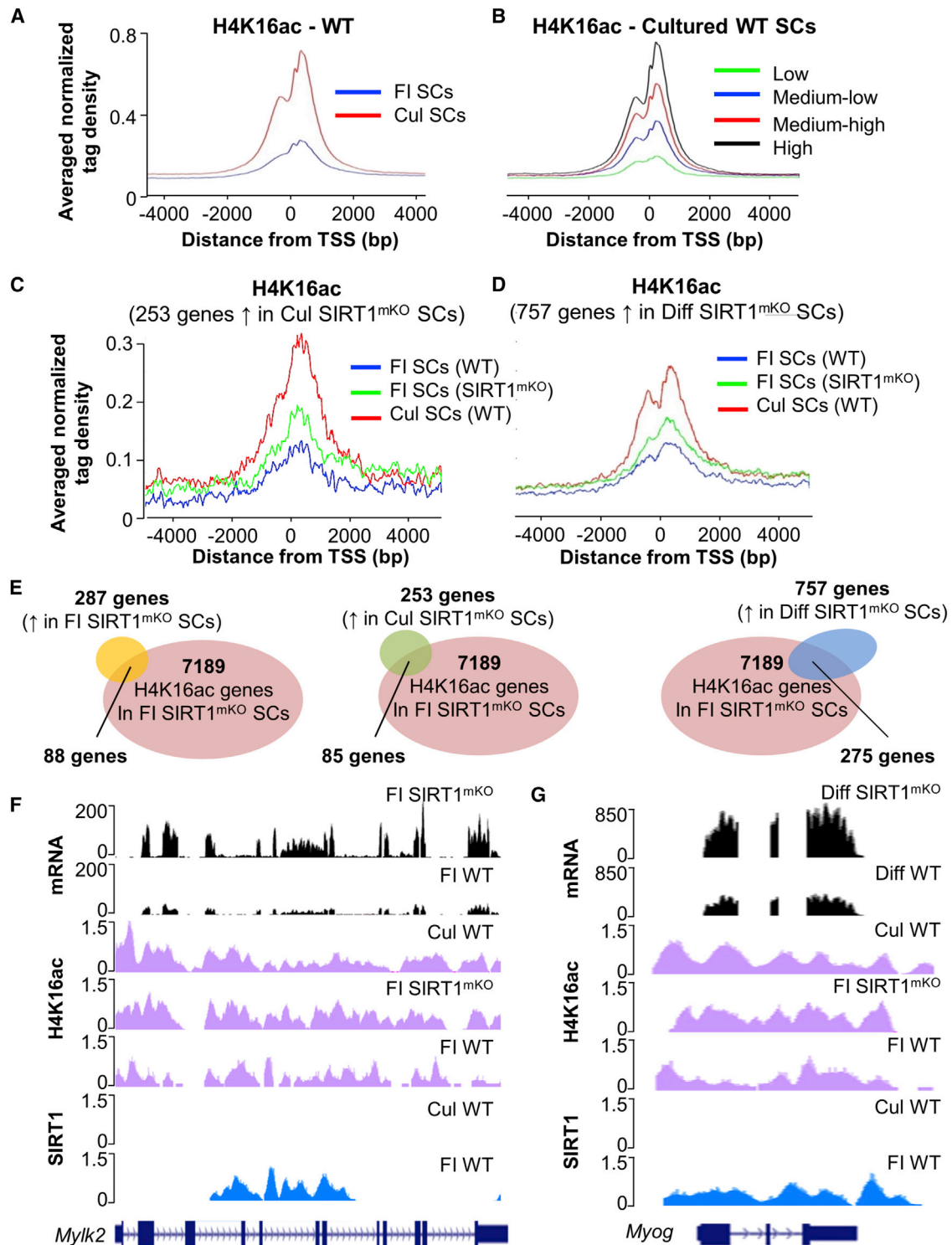


Figure 6. Ablation of the SIRT1 Catalytic Domain Alters H4K16 Acetylation and Influences Expression of Selected Genes

(A) Average signal of normalized tag density for H4K16ac ChIP-seq in FI WT SCs (blue line) and Cul WT SCs (red line).

(B) Average signal of normalized tag density for H4K16ac ChIP-seq in Cul WT SCs for genes with low (green line), medium-low (blue line), medium-high (red line), and high expression (black line).

(C) Average signal of normalized tag density for H4K16ac ChIP-seq in FI WT SCs (blue line), FI *Sirt1*^{mKO} SCs (green line), and Cul WT SCs for genes upregulated in Cul *Sirt1*^{mKO} SCs.

(D) Average signal of normalized tag density for H4K16ac ChIP-seq in FI WT SCs (blue line), FI *Sirt1*^{mKO} SCs (green line), and Cul WT SCs induced to differentiate for genes upregulated in *Sirt1*^{mKO} induced to differentiate.

(legend continued on next page)

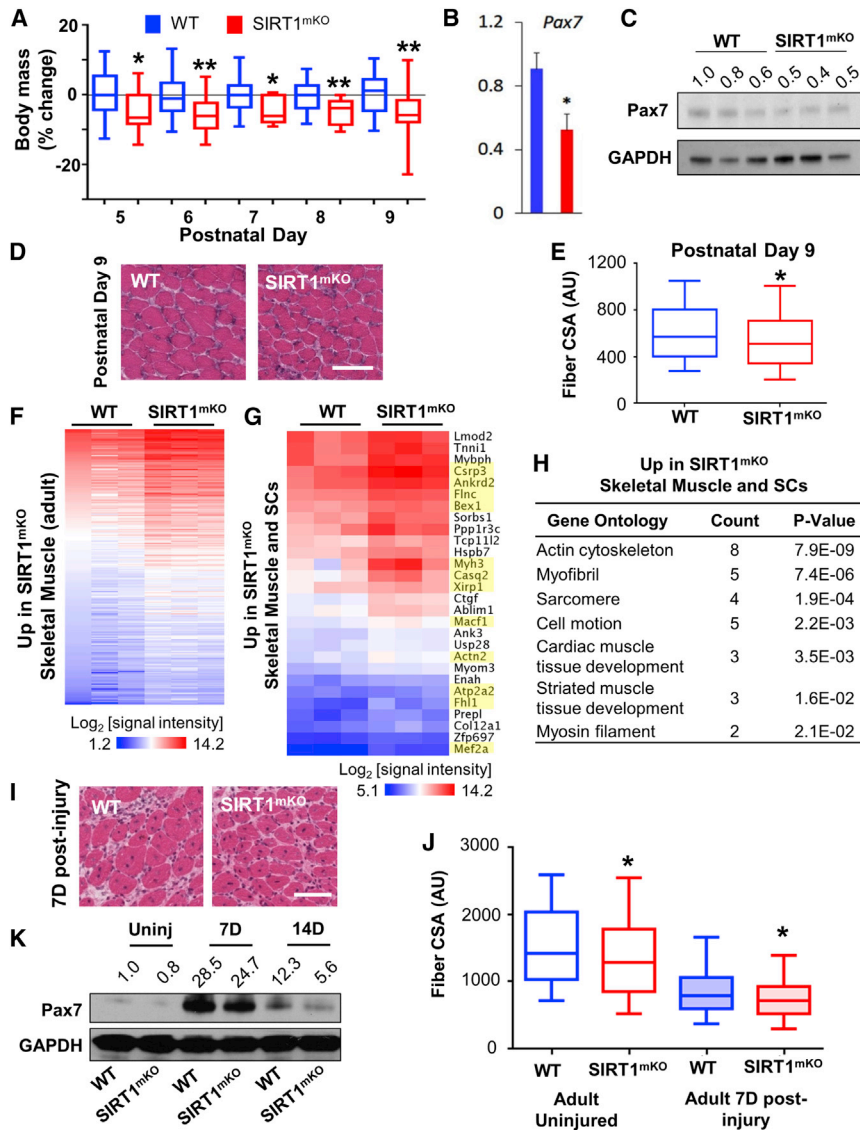


Figure 7. Loss of SIRT1 Deacetylase Activity Leads to Developmental and Regenerative Defects in Skeletal Muscle

(A) Body mass was evaluated starting at postnatal (P) days 5 through 9 in WT and *Sirt1*^{mkKO} mice (WT n = 27; *Sirt1*^{mkKO} = 24). Significance was determined using a Student's t test (two-tailed distribution without assuming equal variance).

(B and C) Pax7 mRNA (left) and protein expression (right) were evaluated in the skeletal muscles of P9 WT and *Sirt1*^{mkKO} mice.

(D) Hematoxylin and eosin (H&E) staining of skeletal muscles in P9 WT and *Sirt1*^{mkKO} mice. White scale bar represents 50 μM.

(E) Quantification of skeletal muscle fiber CSA from P9 mice (>1,000 fibers analyzed/muscle). Results are presented as a box-and-whisker plot. (F) Heatmap of the microarray results (Log₂[signal intensity]) for genes upregulated in *Sirt1*^{mkKO} skeletal muscle. Each gene listed has a mean fold change of >1.5 and p < 0.05 (n = 3 samples/group).

(G) Heatmap of the microarray results (Log₂[signal intensity]) for genes upregulated in both *Sirt1*^{mkKO} SCs induced to differentiate and *Sirt1*^{mkKO} skeletal muscle, with developmentally regulated muscle genes highlighted in yellow.

(H) Gene ontology for genes upregulated in both *Sirt1*^{mkKO} SCs induced to differentiate and *Sirt1*^{mkKO} skeletal muscle.

(I) H&E skeletal muscle staining of 2-month-old (adult) WT and *Sirt1*^{mkKO} mice 7 days after CTX injection.

(J) Quantification of skeletal muscle fiber CSA from adult WT and *Sirt1*^{mkKO} mice regenerating muscles (7 days after CTX, >1,000 fibers analyzed/muscle). Results are presented as a box-and-whisker plot. (K) Pax7 protein levels in uninjured, and 7 and 14 days regenerating muscles of WT and *Sirt1*^{mkKO} mice. Data are presented as mean ± SEM, *p < 0.05; **p < 0.01.

and Rudnicki, 2014). A microarray assay of RNA derived from the gastrocnemius hindlimb muscles revealed an enrichment of 219 and a reduction of 191 transcripts in the muscles of *Sirt1*^{mkKO} compared to WT mice (Figure 7F and Table S5). Of the upregulated transcripts in *Sirt1*^{mkKO} muscle, 28 (corresponding to 12% of the total transcripts) were also increased in *Sirt1*^{mkKO} SCs induced to differentiate (Figure 7G and Table S5). A GO analysis of the transcripts upregulated in both *Sirt1*^{mkKO} muscle and *Sirt1*^{mkKO} SCs returned biological terms related to skeletal muscle development (“myofibril,” “sarcomere,” and “striated muscle development,” Figure 7H). The most highly upregulated transcript in *Sirt1*^{mkKO} muscles corresponded to the embryonic

myosin heavy chain isoform *Myh3* (5.8-fold increase, Table S5), which is physiologically expressed in fetal muscle and repressed in the adult (Weydert et al., 1987). In addition to *Myh3*, several other transcripts upregulated in both *Sirt1*^{mkKO} muscles and *Sirt1*^{mkKO} SCs induced to differentiate are known to be preferentially expressed during muscle development and/or in regenerating muscles (highlighted in Figure 7G, Table S5).

In response to injury, quiescent SCs become activated, enter mitosis, giving rise to myogenic progenitor cells, which ultimately differentiate to restore damaged muscles (Chang and Rudnicki, 2014). To evaluate whether muscle regeneration was altered in

(E) Venn diagram representing genes upregulated in FI *Sirt1*^{mkKO} SCs (287 genes), Cul *Sirt1*^{mkKO} SCs (253 genes), and *Sirt1*^{mkKO} SCs induced to differentiate (757 genes), and genes acquiring H4K16ac in FI *Sirt1*^{mkKO} SCs (7,189 genes).

(F) ChIP-seq and RNA-seq profiles of the *Mylk2* gene. Bottom to top: SIRT1 ChIP-seq profile in FI and Cul WT SCs (blue signals); H4K16ac profile in FI WT and *Sirt1*^{mkKO} SCs (magenta signals); *Mylk2* mRNA expression profile in FI WT and *Sirt1*^{mkKO} SCs (black signals).

(G) ChIP-seq and RNA-seq profiles of the *Myog* gene. Bottom to top: SIRT1 ChIP-seq profile in FI and Cul WT SCs (blue signals); H4K16ac profile in WT and *Sirt1*^{mkKO} FI SCs, and WT Cul SCs (magenta signals); *Myog* mRNA expression profile in FI WT and *Sirt1*^{mkKO} SCs (black signals).

Sirt1^{mkO} mice, muscle damage was induced by injecting the tibialis anterior (TA) muscles of 2-month-old WT or *Sirt1*^{mkO} mice with the myogenic agent cardiotoxin (CTX). Seven days after CTX injection, regenerating muscles of *Sirt1*^{mkO} mice were composed of myofibers with smaller CSA (Figures 7H and 7I), and reduced Pax7 protein (Figure 7J, both at 7 and 14 days after CTX injection), compared to littermate controls. Overall, these findings indicate that SIRT1 is required for appropriate postnatal muscle growth and adult muscle regeneration.

DISCUSSION

In this study, SIRT1 was found to lie at the nexus between SC metabolic reprogramming and muscle gene expression. Our findings are consistent with a model wherein the metabolic state influences the gene expression program of SCs via modulation of the metabolite NAD⁺ and SIRT1 deacetylase activity. Ablation of a SIRT1 domain conferring deacetylase activity resulted in widespread H4K16ac and derepression of several hundred genes in SCs. However, such hyperacetylation did not result in a generalized and immediate transcriptional response of all target genes. For instance, enrichment of H4K16ac at the *Myog* locus was increased in FI *Sirt1*^{mkO} SCs but its expression was augmented only in *Sirt1*^{mkO} SCs induced to differentiate. Local chromatin architecture and additional transcriptional events—including histone dynamics and transcription factor availability—likely determine whether, at specific loci, transcriptional derepression is concomitant with SIRT1 removal or will occur at later stages of cell differentiation. Furthermore, that only approximately 30%–40% of the genes derepressed upon *Sirt1* ablation acquired H4K16ac indicates that either additional histone lysines or nonhistone substrates are involved in SIRT1-mediated transcriptional repression (Houtkooper et al., 2012). It is interesting to note that SIRT1 does not appear to regulate the expression of metabolic regulators. Thus, although SIRT1 responds to the process of SC metabolic reprogramming by influencing H4K16 acetylation and gene expression, it does not play a direct role in the observed switch toward glycolysis in proliferating SCs. Despite the presence of MyoD⁺ SCs on *Sirt1*^{mkO} fibers, the corresponding *Myod1* transcripts were not elevated. This observation is consistent with findings reporting that *Myod1* transcripts are already present in quiescent SCs, not exhibiting a significant increase during SC activation in vivo (Kanisicak et al., 2009; Liu et al., 2013; Pallafacchina et al., 2010; Rodgers et al., 2014). Analogous to microRNA-mediated *Myf5* regulation (Crist et al., 2012), posttranscriptional processing of *Myod1* mRNA transcripts may be responsible for the appearance of the MyoD protein in activated SCs. Moreover, while increased *Myog* transcripts in Cul (24 hr DM) *Sirt1*^{mkO} SCs correlated with the enrichment of H4K16ac at its locus in quiescent *Sirt1*^{mkO} SCs, and SIRT1 disengagement in cultured WT SCs, we cannot exclude that additional regulatory mechanisms controlled by SIRT1 also contribute to *Myog* activation. In this regard, SIRT1 deacetylates the histone acetyltransferases PCAF and p300, and transcription factors MyoD and Foxo3 (Brunet et al., 2004; Fulco et al., 2003; Motta et al., 2004), making it plausible that nonhistone substrates relevant to myogenesis are affected in *Sirt1*^{mkO} SCs. Recently, SIRT1 has been implicated in regulating autophagic flux and SC activation (Tang and Rando,

2014). In this study, autophagy in fiber-associated SCs was detected after 24–36 hr of culture, during which time SCs had entered the S phase of the cell cycle, as measured via an 5-ethynyl-2'-deoxyuridine (EdU) assay. Interestingly, using an inducible SC-specific SIRT1-KO mouse (*Pax7Cre*^{ERT2}*xSirt1*^{fl/fl}), these authors demonstrated that *Sirt1* ablation inhibited autophagic flux and delayed entry into the S phase of the cell cycle. The different timing used to evaluate SC activation, along with the mode of SIRT1 excision (inducible versus constitutive) and the use of MyoD versus EdU as a measure of SC activation, may account for the observed differences between this study and the current results.

Altogether, our findings suggest a role for metabolism in the regulation of SC biology, beyond simply providing the building blocks and ATP required for new cell growth. Within this context, it has previously been shown that the generation of nucleocytoplasmic acetyl-CoA is dependent upon glycolytic production of citrate (Wellen et al., 2009). In contrast, FA oxidation leads to the production of mitochondrial acetyl-CoA for entry into the TCA cycle (Wellen et al., 2009). Thus, any shift toward glycolysis would be expected to lead to both a decrease in SIRT1 deacetylase activity (through reduced NAD⁺), and an increased supply of acetyl-CoA for histone/protein acetylation, and together likely explain the observed increase in global H4K16ac in active SCs. There is previous evidence that the behavior of adult SCs is influenced by regulatory pathways controlled by oxygen tension and metabolic states (Csete et al., 2001; Liu et al., 2012). A link between metabolism and SC function has been proposed, with recent studies indicating a link between OXPHOS and SC clonogenic capacity. Elevated mitochondrial abundance and OXPHOS activity, induced by calorie restriction (CR), was found to be associated with an increase in the number of cells capable of initiating myogenic colony formation (Cerletti et al., 2012). Regulation of MyoD and Myogenin by increased SIRT1 activity elicited by CR would keep SCs in a stem-like state and favor their clonogenicity. Consistent with this, both the SIRT1 level and the metabolic milieu conducive to its activation were augmented in SCs derived from CR animals (Cerletti et al., 2012). A similar increase in clonogenic capacity was observed in HSC with increased FA oxidation (Ito et al., 2012) while, more recently, glucose and glutamine metabolism has been reported to regulate human HSC lineage specification (Oburoglu et al., 2014).

Finally, our gene expression profiling of whole muscles revealed deregulated transcription in *Sirt1*^{mkO} mice. Intriguingly, a subset of the upregulated transcripts was also increased in *Sirt1*^{mkO} SCs induced to differentiate (Figure 7G). Because in adult mice SCs have completed their differentiation process to give rise to mature myofibers, we interpret these findings to indicate that the upregulated transcripts identified in *Sirt1*^{mkO} muscles derive from the myofiber compartment. The presence of such transcripts in both differentiating *Sirt1*^{mkO} SCs and *Sirt1*^{mkO} adult muscles suggests that their deregulation likely originates in SCs and is further maintained in the adult muscle.

In summary, our results provide insights into the developing paradigm linking the process of metabolic reprogramming, transcriptional regulation, and acquisition of defined cell states. In the absence of SIRT1, quiescent SCs lose their respective blueprint of carefully regulated H4K16ac and undergo a progressive deregulation of gene expression during activation and

differentiation. We conclude that metabolic modifications affect the activity of SIRT1, which acts as a relay able to interpret the rapid change in metabolism (via NAD⁺) and induce subsequent changes in H4K16 acetylation status and gene expression.

EXPERIMENTAL PROCEDURES

Full details are provided in the [Supplemental Experimental Procedures](#).

Fluorescence-Activated Cell Sorting

SCs were sorted based on our previously described technique (Juan et al., 2011), which utilizes a modified version of the method described by Kuang et al. (2007). Briefly, hindlimb muscles from mice were digested with 0.2% collagenase for 60 min and SCs were liberated by treating the resultant slurry with collagenase/dispase. All cells were incubated with primary antibodies raised against α 7-integrin, and PE-labeled CD11, CD31, CD45, and Sca1, and Hoechst 33342 (10 μ g/ml) and PI (30 min). SCs were isolated via FACS, gating on positive α 7-integrin and Hoechst staining, and negative PI and PE-CD/11/CD31/CD45/Sca1 staining.

Single Muscle Fiber Isolation and Culture

Single EDL fibers were isolated and cultured as previously described (Juan et al., 2011). Briefly, single fibers were liberated in a collagenase solution and then immediately fixed in 4% paraformaldehyde, or cultured in growth media for the specified time (see [Supplemental Experimental Procedures](#) for growth media conditions). Measurements of relative fluorescent units (RFU) were completed via ImageJ (NIH) and represent gray intensity multiplied by nuclear size (see [Supplemental Experimental Procedures](#) for details).

Chromatin Immunoprecipitation

For ChIP-seq, $\sim 1 \times 10^6$ SCs (isolated via FACS from the hindlimbs of seven to eight mice) were immediately crosslinked (for FI SCs) or cultured for 48 hr (Cul SCs) and subsequently crosslinked in 1% formaldehyde and processed according to published protocols (Métivier et al., 2003; Mousavi et al., 2012). Briefly, cells were lysed in RIPA buffer (1 \times PBS, 1% NP-40, 0.5% sodium deoxycholate, 0.1% SDS) and centrifuged at 2,000 revolutions per minute for 5 min. The chromatin fraction was sheared by sonication (4 \times 30sec) in 1.5 ml siliconized Eppendorf tubes. The resulting sheared chromatin samples were cleared for 1 hr, immunoprecipitated overnight, and washed in buffer I (20 mM TrisHCl [pH 8.0], 150 mM NaCl, 2 mM EDTA, 0.1% SDS, 1% Triton X-100), buffer II (20 mM TrisHCl [pH 8.0], 500 mM NaCl, 2 mM EDTA, 0.1% SDS, 1% Triton X-100), buffer III (10 mM TrisHCl [pH 8.0], 250 mM LiCl, 1% NP-40; 1% sodium deoxycholate, 1 mM EDTA), and Tris-EDTA (pH 8.0). All washes were performed at 4°C for 5 min. Finally, crosslinking was reversed in elution buffer (100 mM sodium bicarbonate [NaHCO₃], 1% SDS) at 65°C overnight.

Cellular Bioenergetics

Oxygen consumption and extracellular acidification rates of both SCs and C2C12 cells were measured on an extracellular flux bioanalyzer (XF96, Seahorse Biosciences), and seeded at a density of 50,000 and 12,000 cells per well, respectively (see [Supplemental Experimental Procedures](#) for details).

Mice

The initial characterization of the metabolic profile of SCs was conducted in WT mice (C57BL/6 background). *Sirt1*^{tmKO} mice were generated via breeding of Pax7^{cre/+} knockin mice (Keller et al., 2004) with mice containing the floxed exon 4 *Sirt1* allele (Li et al., 2007). Skeletal muscle injury was induced via a single intramuscular injection of the snake venom cardiotoxin to the TA muscle. Briefly, cardiotoxin (20 μ g/ml) was injected into the TA muscle until the maximal holding capacity of the muscle was reached (30–50 μ l). In all cases using *Sirt1*^{tmKO} mice, littermates were used as controls. All experiments were performed according to the NIH Animal Care and Use regulations.

Statistical Analyses

All data are presented as mean \pm SEM, excluding RFU measurements of H4K16ac and MyoD and muscle fiber CSA, which are expressed as box-and-whisker plots. Statistical analyses were performed using a Student's t test to calculate differences between two groups, or a two-way ANOVA followed by a Tukey's post hoc analysis for multiple comparisons. For data presented as box-and-whisker plots, data were determined to be statistically different when the median \pm 95% CI did not overlap.

ACCESSION NUMBERS

The Gene Expression Omnibus accession number for RNA-seq and ChIP-seq datasets reported in this paper is GSE64379.

SUPPLEMENTAL INFORMATION

Supplemental Information includes Supplemental Experimental Procedures, seven figures, and five tables and can be found with this article online at <http://dx.doi.org/10.1016/j.stem.2014.12.004>.

AUTHOR CONTRIBUTIONS

J.G.R., S.D., and V.S. designed the experiments and wrote the manuscript. J.G.R. performed most of the presented experiments. S.D. performed RNA-seq and ChIP-seq experiments. A.D. performed FACS and RNA-seq experiments. A.J. performed single fiber isolation and immunofluorescence staining. H.Z. conducted bioinformatics analysis of RNA-seq and ChIP-seq data. X.F. performed muscle injury experiments, muscle sectioning, and immunofluorescence staining and helped with animal breeding. D.C. performed FACS experiments. M.K. supervised animal breeding and analyzed animal body mass. G.G.-C. prepared libraries for RNA-seq and ChIP-seq and performed sequencing. M.F. provided technical and intellectual advice.

ACKNOWLEDGMENTS

We thank Yansong Gu (University of Washington, Seattle) for sharing the *Sirt1* floxed mice, Kristina Zaal (Light Imaging Section, National Institute of Arthritis and Musculoskeletal and Skin Diseases [NIAMS]) for help in evaluating Pax7⁺/MyoD⁺ immunofluorescence staining, and Jim Simone (Flow Cytometry Section, NIAMS) for help with FACS. J.G.R. was supported, in part, via an Overseas Biomedical Research Fellowship from the National Health & Medical Research Council of Australia. This work was supported by the Intramural Research Program of NIAMS at the NIH.

Received: November 19, 2013

Revised: August 27, 2014

Accepted: December 16, 2014

Published: January 15, 2015

REFERENCES

- Abe, S., Hirose, D., Kado, S., Iwanuma, O., Saka, H., Yanagisawa, N., and Ide, Y. (2009). Increased expression of decorin during the regeneration stage of mdx mouse. *Anat. Sci. Int.* **84**, 305–311.
- Brack, A.S., and Rando, T.A. (2012). Tissue-specific stem cells: lessons from the skeletal muscle satellite cell. *Cell Stem Cell* **10**, 504–514.
- Brunet, A., Sweeney, L.B., Sturgill, J.F., Chua, K.F., Greer, P.L., Lin, Y., Tran, H., Ross, S.E., Mostoslavsky, R., Cohen, H.Y., et al. (2004). Stress-dependent regulation of FOXO transcription factors by the SIRT1 deacetylase. *Science* **303**, 2011–2015.
- Cerletti, M., Jang, Y.C., Finley, L.W., Haigis, M.C., and Wagers, A.J. (2012). Short-term calorie restriction enhances skeletal muscle stem cell function. *Cell Stem Cell* **10**, 515–519.
- Chang, N.C., and Rudnicki, M.A. (2014). Satellite cells: the architects of skeletal muscle. *Curr. Top. Dev. Biol.* **107**, 161–181.

- Collins, C.A., and Zammit, P.S. (2009). Isolation and grafting of single muscle fibres. *Methods Mol. Biol.* *482*, 319–330.
- Crist, C.G., Montarras, D., and Buckingham, M. (2012). Muscle satellite cells are primed for myogenesis but maintain quiescence with sequestration of Myf5 mRNA targeted by microRNA-31 in mRNP granules. *Cell Stem Cell* *11*, 118–126.
- Csete, M., Walikonis, J., Slawny, N., Wei, Y., Korsnes, S., Doyle, J.C., and Wold, B. (2001). Oxygen-mediated regulation of skeletal muscle satellite cell proliferation and adipogenesis in culture. *J. Cell. Physiol.* *189*, 189–196.
- Dentice, M., Marsili, A., Ambrosio, R., Guardiola, O., Sibilio, A., Paik, J.H., Minchiotti, G., DePinho, R.A., Fenzi, G., Larsen, P.R., and Salvatore, D. (2010). The FoxO3/type 2 deiodinase pathway is required for normal mouse myogenesis and muscle regeneration. *J. Clin. Invest.* *120*, 4021–4030.
- Dey, B.K., Pfeifer, K., and Dutta, A. (2014). The H19 long noncoding RNA gives rise to microRNAs miR-675-3p and miR-675-5p to promote skeletal muscle differentiation and regeneration. *Genes Dev.* *28*, 491–501.
- Fukada, S., Uezumi, A., Ikemoto, M., Masuda, S., Segawa, M., Tanimura, N., Yamamoto, H., Miyagoe-Suzuki, Y., and Takeda, S. (2007). Molecular signature of quiescent satellite cells in adult skeletal muscle. *Stem Cells* *25*, 2448–2459.
- Fulco, M., Schiltz, R.L., Iezzi, S., King, M.T., Zhao, P., Kashiwaya, Y., Hoffman, E., Veech, R.L., and Sartorelli, V. (2003). Sir2 regulates skeletal muscle differentiation as a potential sensor of the redox state. *Mol. Cell* *12*, 51–62.
- Goetsch, S.C., Martin, C.M., Embree, L.J., and Garry, D.J. (2005). Myogenic progenitor cells express filamin C in developing and regenerating skeletal muscle. *Stem Cells Dev.* *14*, 181–187.
- Gohil, V.M., Sheth, S.A., Nilsson, R., Wojtovich, A.P., Lee, J.H., Perocchi, F., Chen, W., Clish, C.B., Ayata, C., Brookes, P.S., and Mootha, V.K. (2010). Nutrient-sensitized screening for drugs that shift energy metabolism from mitochondrial respiration to glycolysis. *Nat. Biotechnol.* *28*, 249–255.
- Grifone, R., Demignon, J., Giordani, J., Niro, C., Souil, E., Bertin, F., Laclef, C., Xu, P.X., and Maire, P. (2007). Eya1 and Eya2 proteins are required for hypaxial somitic myogenesis in the mouse embryo. *Dev. Biol.* *302*, 602–616.
- Guarente, L. (2000). Sir2 links chromosome silencing, metabolism, and aging. *Genes Dev.* *14*, 1021–1026.
- Guarente, L. (2011). Sirtuins, aging, and metabolism. *Cold Spring Harb. Symp. Quant. Biol.* *76*, 81–90.
- Houtkooper, R.H., Pirinen, E., and Auwerx, J. (2012). Sirtuins as regulators of metabolism and healthspan. *Nat. Rev. Mol. Cell Biol.* *13*, 225–238.
- Imai, S., Armstrong, C.M., Kaebertlein, M., and Guarente, L. (2000). Transcriptional silencing and longevity protein Sir2 is an NAD-dependent histone deacetylase. *Nature* *403*, 795–800.
- Ito, K., Carracedo, A., Weiss, D., Arai, F., Ala, U., Avigan, D.E., Schafer, Z.T., Evans, R.M., Suda, T., Lee, C.H., and Pandolfi, P.P. (2012). A PML-PPAR- δ pathway for fatty acid oxidation regulates hematopoietic stem cell maintenance. *Nat. Med.* *18*, 1350–1358.
- Jeong, J., Conboy, M.J., and Conboy, I.M. (2013). Pharmacological inhibition of myostatin/TGF- β receptor/pSmad3 signaling rescues muscle regenerative responses in mouse model of type 1 diabetes. *Acta Pharmacol. Sin.* *34*, 1052–1060.
- Juan, A.H., Derfoul, A., Feng, X., Ryall, J.G., Dell'Orso, S., Pasut, A., Zare, H., Simone, J.M., Rudnicki, M.A., and Sartorelli, V. (2011). Polycomb EZH2 controls self-renewal and safeguards the transcriptional identity of skeletal muscle stem cells. *Genes Dev.* *25*, 789–794.
- Kanisicak, O., Mendez, J.J., Yamamoto, S., Yamamoto, M., and Goldhamer, D.J. (2009). Progenitors of skeletal muscle satellite cells express the muscle determination gene, MyoD. *Dev. Biol.* *332*, 131–141.
- Katada, S., Imhof, A., and Sassone-Corsi, P. (2012). Connecting threads: epigenetics and metabolism. *Cell* *148*, 24–28.
- Keller, C., Hansen, M.S., Coffin, C.M., and Capecchi, M.R. (2004). Pax3:Fkhr interferes with embryonic Pax3 and Pax7 function: implications for alveolar rhabdomyosarcoma cell of origin. *Genes Dev.* *18*, 2608–2613.
- Koo, J.H., Smiley, M.A., Lovering, R.M., and Margolis, F.L. (2007). Bex1 knock out mice show altered skeletal muscle regeneration. *Biochem. Biophys. Res. Commun.* *363*, 405–410.
- Kuang, S., Kuroda, K., Le Grand, F., and Rudnicki, M.A. (2007). Asymmetric self-renewal and commitment of satellite stem cells in muscle. *Cell* *129*, 999–1010.
- Kuang, S., Gillespie, M.A., and Rudnicki, M.A. (2008). Niche regulation of muscle satellite cell self-renewal and differentiation. *Cell Stem Cell* *2*, 22–31.
- Li, H., Rajendran, G.K., Liu, N., Ware, C., Rubin, B.P., and Gu, Y. (2007). SirT1 modulates the estrogen-insulin-like growth factor-1 signaling for postnatal development of mammary gland in mice. *Breast Cancer Res.* *9*, R1.
- Liu, W., Wen, Y., Bi, P., Lai, X., Liu, X.S., Liu, X., and Kuang, S. (2012). Hypoxia promotes satellite cell self-renewal and enhances the efficiency of myoblast transplantation. *Development* *139*, 2857–2865.
- Liu, L., Cheung, T.H., Charville, G.W., Hurgo, B.M., Leavitt, T., Shih, J., Brunet, A., and Rando, T.A. (2013). Chromatin modifications as determinants of muscle stem cell quiescence and chronological aging. *Cell Rep.* *4*, 189–204.
- Lu, C., and Thompson, C.B. (2012). Metabolic regulation of epigenetics. *Cell Metab.* *16*, 9–17.
- Lunt, S.Y., and Vander Heiden, M.G. (2011). Aerobic glycolysis: meeting the metabolic requirements of cell proliferation. *Annu. Rev. Cell Dev. Biol.* *27*, 441–464.
- Métivier, R., Penot, G., Hübner, M.R., Reid, G., Brand, H., Kos, M., and Gannon, F. (2003). Estrogen receptor- α directs ordered, cyclical, and combinatorial recruitment of cofactors on a natural target promoter. *Cell* *115*, 751–763.
- Michan, S., and Sinclair, D. (2007). Sirtuins in mammals: insights into their biological function. *Biochem. J.* *404*, 1–13.
- Motta, M.C., Divecha, N., Lemieux, M., Kamel, C., Chen, D., Gu, W., Bultsma, Y., McBurney, M., and Guarente, L. (2004). Mammalian SIRT1 represses forkhead transcription factors. *Cell* *116*, 551–563.
- Mousavi, K., Zare, H., Wang, A.H., and Sartorelli, V. (2012). Polycomb protein Ezh1 promotes RNA polymerase II elongation. *Mol. Cell* *45*, 255–262.
- Oburoglu, L., Tardito, S., Fritz, V., de Barros, S.C., Merida, P., Craveiro, M., Mamede, J., Cretenet, G., Mongellaz, C., An, X., et al. (2014). Glucose and glutamine metabolism regulate human hematopoietic stem cell lineage specification. *Cell Stem Cell* *15*, 169–184.
- Ono, Y., Calhabeu, F., Morgan, J.E., Katagiri, T., Amthor, H., and Zammit, P.S. (2011). BMP signalling permits population expansion by preventing premature myogenic differentiation in muscle satellite cells. *Cell Death Differ.* *18*, 222–234.
- Pallafacchina, G., François, S., Regnault, B., Czarny, B., Dive, V., Cumano, A., Montarras, D., and Buckingham, M. (2010). An adult tissue-specific stem cell in its niche: a gene profiling analysis of in vivo quiescent and activated muscle satellite cells. *Stem Cell Res. (Amst.)* *4*, 77–91.
- Rodgers, J.T., Lerin, C., Haas, W., Gygi, S.P., Spiegelman, B.M., and Puigserver, P. (2005). Nutrient control of glucose homeostasis through a complex of PGC-1 α and SIRT1. *Nature* *434*, 113–118.
- Rodgers, J.T., King, K.Y., Brett, J.O., Cromie, M.J., Charville, G.W., Maguire, K.K., Brunson, C., Mastey, N., Liu, L., Tsai, C.R., et al. (2014). mTORC1 controls the adaptive transition of quiescent stem cells from G0 to G(Alert). *Nature* *510*, 393–396.
- Ryall, J.G. (2012). The role of sirtuins in the regulation of metabolic homeostasis in skeletal muscle. *Curr. Opin. Clin. Nutr. Metab. Care* *15*, 561–566.
- Ryall, J.G. (2013). Metabolic reprogramming as a novel regulator of skeletal muscle development and regeneration. *FEBS J.* *280*, 4004–4013.
- Sauve, A.A., and Youn, D.Y. (2012). Sirtuins: NAD(+)-dependent deacetylase mechanism and regulation. *Curr. Opin. Chem. Biol.* *16*, 535–543.
- Shea, K.L., Xiang, W., LaPorta, V.S., Licht, J.D., Keller, C., Basson, M.A., and Brack, A.S. (2010). Sprouty1 regulates reversible quiescence of a self-renewing adult muscle stem cell pool during regeneration. *Cell Stem Cell* *6*, 117–129.

- Shogren-Knaak, M., Ishii, H., Sun, J.M., Pazin, M.J., Davie, J.R., and Peterson, C.L. (2006). Histone H4-K16 acetylation controls chromatin structure and protein interactions. *Science* 311, 844–847.
- Shyh-Chang, N., Daley, G.Q., and Cantley, L.C. (2013). Stem cell metabolism in tissue development and aging. *Development* 140, 2535–2547.
- Tajbakhsh, S. (2009). Skeletal muscle stem cells in developmental versus regenerative myogenesis. *J. Intern. Med.* 266, 372–389.
- Tang, A.H., and Rando, T.A. (2014). Induction of autophagy supports the bioenergetic demands of quiescent muscle stem cell activation. *EMBO J.* 33, 2782–2797.
- Taylor, G.C., Eskeland, R., Hekimoglu-Balkan, B., Pradeepa, M.M., and Bickmore, W.A. (2013). H4K16 acetylation marks active genes and enhancers of embryonic stem cells, but does not alter chromatin compaction. *Genome Res.* 23, 2053–2065.
- Vaquero, A., Scher, M., Lee, D., Erdjument-Bromage, H., Tempst, P., and Reinberg, D. (2004). Human SirT1 interacts with histone H1 and promotes formation of facultative heterochromatin. *Mol. Cell* 16, 93–105.
- Wellen, K.E., Hatzivassiliou, G., Sachdeva, U.M., Bui, T.V., Cross, J.R., and Thompson, C.B. (2009). ATP-citrate lyase links cellular metabolism to histone acetylation. *Science* 324, 1076–1080.
- Weydert, A., Barton, P., Harris, A.J., Pinset, C., and Buckingham, M. (1987). Developmental pattern of mouse skeletal myosin heavy chain gene transcripts in vivo and in vitro. *Cell* 49, 121–129.
- Yin, H., Price, F., and Rudnicki, M.A. (2013). Satellite cells and the muscle stem cell niche. *Physiol. Rev.* 93, 23–67.
- Zhou, W., Choi, M., Margineantu, D., Margaretha, L., Hesson, J., Cavanaugh, C., Blau, C.A., Horwitz, M.S., Hockenbery, D., Ware, C., and Ruohola-Baker, H. (2012). HIF1 α induced switch from bivalent to exclusively glycolytic metabolism during ESC-to-EpiSC/hESC transition. *EMBO J.* 31, 2103–2116.